THE JOURNAL OF PHYSICAL CHEMISTRY A

 VOLUME 108, NUMBER 14, APRIL 8, 2004

ARTICLES

Rotamer Dynamics of Substituted Simple Alkanes. 1. A Classical Trajectory Study of Collisional Orientation and Alignment of 1-Bromo-2-Chloroethane with Argon

H.-N. Lee and T.-M. Su*

Department of Chemistry, National Taiwan University, Taipei, Taiwan, and Institute of Atomic and Molecular Sciences, Academia Sinica, Taipei, Taiwan

I. Chao*

Institute of Chemistry, Academia Sinica, Taipei, Taiwan

Received: October 29, 2003; In Final Form: January 11, 2004

The 1-bromo-2-chloroethane molecule could exist in T, G, and G′ rotamer forms. The collisional orientation and alignment of these rotamers in colliding with the Ar atom were studied by classical trajectory method. With the initial translational collision energies and rotational energies being selected in the main energy range covered by room temperatures to around 1000 K, the collisional orientation and alignment moments of the rotamers of the title molecule were calculated as a function of the impact parameter and the rotational angular momentum along the molecular *z* axis. As far as the collisional orientation and alignment behaviors are concerned, the calculations show that there are similarities as well as differences between these rotamers. Following the generally accepted physical models developed for the collisional alignment of diatomic molecules, model mechanisms for the collisional orientation and alignment of the present system were proposed and discussed.

1. Introduction

The collisional alignment and/or orientation of molecules in a directed flow have been known to play an important role in the macroscopic transport processes of nonspherical molecules in gases since the 1960s.[1] With the advent of molecule beam and laser excitation/fluorescence detection techniques in the 1970s, this subject has been under intensive theoretical and experimental studies for more than two decades now.[2−22] Recent progress in this direction has demonstrated that the aligned molecules could be used to probe the anisotropy of the interaction potential surfaces between the collisional partners.[23] Besides, the capability of generating a high-intensity beam of aligned and/or oriented molecules opens new possibilities in the dynamics study of stereospecific chemical reactions.[21−23] Experimentally, under the supersonic expansion condition of a molecular beam, the aligned distributions of seeded rotor molecules were studied for Na_2,[2,5,9] I_2,[4,7,8,10,11] CO_2,[12] CO,[17] O_2,[13,14] N_2,[18] and C_6H_6 (benzene).[21,22] In a different approach, with the flow-drift method, the rotational alignment of N_2^+ drifted in He was reported.[6,16] Theoretically, in an earlier effort, the rotational alignment of I_2 in colliding with Ar was analyzed by simple collision models and classical trajectory calculations.[3,15] Further on, the molecular alignment of the O_2/He system was studied quantum mechanically.[19] Detailed alignment and rotational cooling mechanisms were elaborated at the single-molecular collision level. Following up, the collisional alignments of CO/He, O_2/He, and CO_2/He in supersonic expansions were simulated by the classical trajectory calculations.[20] The

* Authors to whom correspondence may be addressed.

10.1021/jp037260y CCC: $27.50
Published on Web 03/12/2004

effect of the multiple collisions on the alignment moments was specifically examined in this recent study.[20]

Up to date, the collisional alignment and/or orientation of nonspherical molecules have been limited to small systems, such as CO and CO_2, or rigid ones, such as C_6H_6. Molecular systems with internal rotations, such as the simple 1-bromo-2-chloroethane (BC) molecule, have not been addressed. These systems are interesting because, say at room temperatures, they are usually populated in several rotamer states. The physical and chemical properties of these rotamers are different from each other. In colliding with an incoming atom or molecule, it is expected that these rotamers would manifest different collisional alignment and/or orientation distributions. In this report, the collisional alignment and orientation of BC in colliding with Ar were studied by the classical trajectory calculations. The distinctive dynamic behaviors of the rotamers and the collisional alignment and/or orientation mechanisms were addressed in this work. This is the first of a series of studies on the rotamer dynamics of substituted simple alkanes embarked in this lab. In the second study of this sequel, the preferential excitation of the conformational energies among the oriented G, G′, and T rotamers of BC as they collide with a surface shall be reported. Other related studies on different substituted alkanes and colliding partners and experimental observations of these collisional effects under a directed flow condition shall be followed.

2. Computational Approach

Conformational Potential of 1-Bromo-2-chloroethane. The ab initio conformational potential of the BC molecule was calculated by the Gaussian 98 software package.[24] For a given dihedral angle of Cl−C−C−Br, the geometry of the molecule was optimized at the MP2(full)/6-31G(d,p) level. The corresponding single-point energy was then calculated at the MP2(full)/6-311+G(2d,p) level. Panel a of Figure 1 shows the ball-and-stick molecular models of the G and T rotamers of BC, and panel b shows the ab initio conformational potential as a function of the ClCCBr dihedral angle. Three local minima were located and designated as G, T, and G′ rotamers. The global conformational potential, the equilibrium geometries, and harmonic vibrational frequencies of the stable rotamers were used as references in fine tuning the molecular force constants to be used in the trajectory calculations. The details are described in the following subsection.

Potential Energy Surfaces. Since the basic trajectory calculations were carried out by the Venus96 chemical dynamics computer program,[25] the potential energy surfaces were constructed from its built-in potential-energy functions. Table 1 lists the functional forms of the interaction potentials adapted in this study. In brief, the potential surface of the BC molecule itself was consisted of the functions of Morse stretch, harmonic bend, generalized exponential repulsion and attraction, nondiagonal stretch−bend interaction, nondiagonal bend−bend interaction, and torsion for dihedral angles. For the interactions between Ar and BC, the generalized exponential repulsion and attraction potentials between the argon atom and the individual BC atoms were employed. There are one-to-one correspondences between these potential functional forms and those employed in the MM3(94) force field.[26] In this report, the force-field parameters were adapted directly from those of MM3 except for the parameters described as follows. Since the stretching function of the MM3 is expressed in polynomial form, the parameters of the Morse stretching function were obtained by equating the expanded polynomial form to that of the MM3. The harmonic

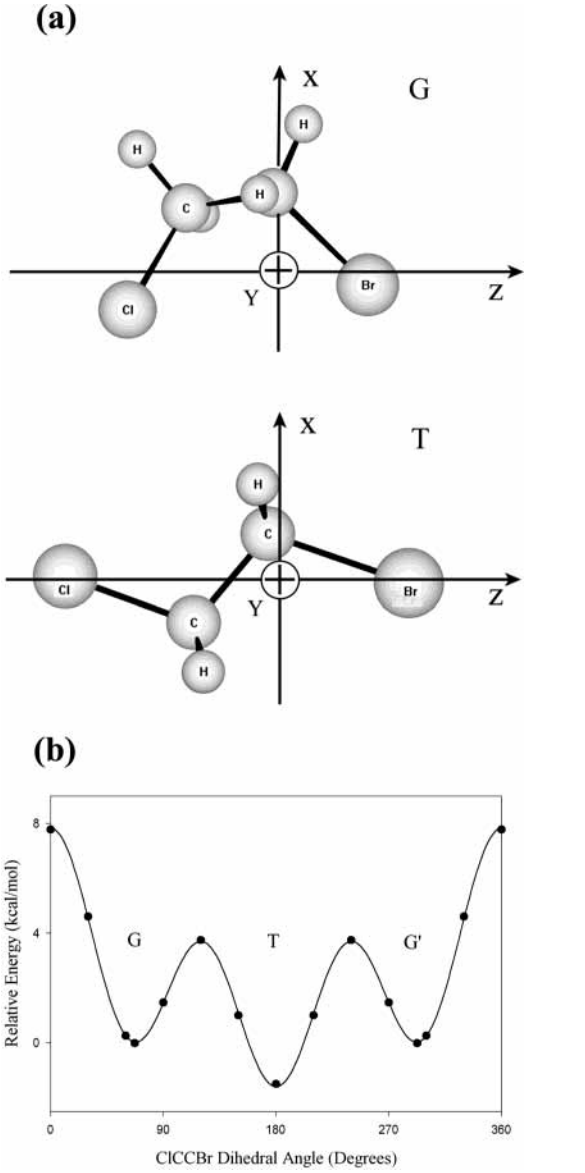

Figure 1. (a) Ball-and-stick representations of the G and T rotamers and their principal axes defined in this report. (b) Conformational potential of 1-bromo-2-chloroethane obtained by the ab initio molecular calculations at the MP2(full)6-311+G(2d,p) level. Three rotamers, G, G′, and T, are indicated.

TABLE 1: Functional Forms of the Interaction Potentials

type of interaction	functional form[a]
Morse stretch	$D(1 - \exp(-\beta\Delta r))^2$
harmonic bend	$(1/2)f_\theta^0(\theta - \theta_0)^2$
exponential repulsion and attraction	$a\exp(-br) + c/r^6$
stretch−bend interaction	$f_{r\theta}^0(r_{ij} - r_{ij}^0)(\theta_k - \theta_k^0)$
bend−bend interaction	$f_{\theta\theta'}^0(\theta_{ijk} - \theta_{ijk}^0)(\theta_{lmn} - \theta_{lmn}^0)$
torsion for dihedral angle	$\sum_{n=1}^{3}(k_d^n/2)(1 + \cos(n\varphi - \gamma_n))$

[a] The symbols D, β, f_θ^0, θ_0, a, b, c, $f_{r\theta}^0$, r_{ij}^0, θ_k^0, $f_{\theta\theta'}^0$, θ_{ijk}^0, k_d^n, and γ_n are the constant parameters used in the force field.

vibrational frequencies calculated with the recommended MM3 constant parameters are consistently lower than those of the ab initio values. The force constants of the stretching and bending motions of the MM3 were scaled up by a factor of 1.153 to improve their agreement. The equilibrium bond lengths were adjusted to fit the ab initio values. Finally, the constant force-

field parameters of the torsional potential of the ClCCBr dihedral angle were fine tuned to fit the global ab initio conformational potential as shown in Figure 1. The final global conformational potential of BC obtained by the force field agrees with the ab initio one to within 0.05 kcal/mol. The constant parameters of the force field which are employed for the present calculations are listed in the Supporting Information section.

It has been well recognized that, in elucidating an elementary chemical reaction, it is essential to acquire an accurate global potential-energy surface for the whole process.[27,28] To simulate the deceptively simple S_N2 nucleophilic substitution reactions of $Cl^- + CH_3Cl$ and $Cl^- + CH_3Br$, it has been demonstrated that the obtaining of accurate global analytic potential surfaces for polyatomic molecules is no mean task.[27,28] The present BC molecule is apparently much more complex than the above halomethanes. The related calculations to obtain a comprehensive global analytic potential surface are expected to be much more involved. Nevertheless, in the present study, only the collisional alignment and orientation of low internal energy states are studied. Those channels that are involved in the rearrangement of bonded atoms are not addressed in this work. It is reckoned that the potential-energy surface of BC + Ar developed in this section, which has only been fine tuned to the equilibrium geometry, vibrational frequencies, and conformational energy, is adequate for the present purpose if the total internal energy of BC + Ar is kept below 20 kcal/mol.

Trajectory Calculations. Panel a of Figure 1 shows the Cartesian coordinates of the principal axes for the G and T rotamers of BC defined in this study. The moments of inertia along the principal axes are $I_x = 337.0$, $I_y = 377.5$, and $I_z = 57.8$ amu Å^2 for the G rotamer and $I_x = 519.6$, $I_y = 530.4$, and $I_z = 17.4$ amu Å^2 for the T rotamer, respectively. Apparently, both rotamers are near-symmetric top molecules. The rotational quantum number along the molecular *z* axis is not an exact good quantum number but is a good approximation for the present case. In this report, the rotational states of the rotamers are described by the language of a symmetric top. Note that in this study, the rotational state information was always extracted through full trajectory calculations of the rotational motions of the rotamers.

For the BC molecule, the molecular backbone vector is defined by the positional vector of the two carbon atoms, $\mathbf{r}_{CC} = \mathbf{r}_{C(Br)} - \mathbf{r}_{C(Cl)}$, in which $\mathbf{r}_{C(Br)}$ is the positional vector of the carbon atom bonded to the bromine atom and $\mathbf{r}_{C(Cl)}$is that bonded to the chlorine atom. In the Ar/BC collision process, the initial relative velocity of Ar with respect to BC is defined by $\mathbf{v} = \mathbf{v}_{Ar} - \mathbf{v}_{BC}$, in which $\mathbf{v}_{BC}$is the velocity of the center of mass of BC.

As mentioned previously, the basic calculations were carried out by the Venus96 general chemical dynamics computer program.[25] To meet a number of specific requirements for the present study, minor modifications were made in the program sections dealing with the defining of the initial collision conditions and the information extracting of the final states. In a routine calculation, for a given total rotational energy of BC, the rotational energy along the *z* axis was then selected from the allowed range of 0 to full value of the total rotational energy. The remaining rotational energy was then equally divided between the rotational motions along the *x* and *y* axes. In this way, the rotational states of BC were specified in terms of the rotational angular momentum **j** and the rotational angular momentum along the *z* axis, $\pm j_z$. For most of the calculations in this study, the normal-mode vibrational energies were set at zero. Finally, the relative collision conditions between Ar and BC were defined by the translational collision energy and the impact parameter. In summary, for a specific set of the above-mentioned parameters, a randomly oriented BC molecule was then selected and a full trajectory was calculated. In this report, a minimum of 5000 trajectories was taken to obtain the average physical quantities over the orientation of the BC molecule.

The initial relative velocity **v** and the final carbon−carbon position vector $\mathbf{r}_{CC}$ after the collision would define a polar angle θ. The probability density of BC with its $\mathbf{r}_{CC}$ pointing at an angle θ with respect to the initial relative velocity **v** can be described by an expansion in Legendre polynomials[10,15,20]

$$\rho(\cos\theta) = (^1/_2)(1 + a_1P_1(\cos\theta) + a_2P_2(\cos\theta) + ...) \quad (1)$$

The expansion coefficients $a_n$can be obtained from

$$a_n = (2n+1)\langle P_n(\cos\theta)\rangle = \frac{(2n+1)}{N_{traj}}\sum_{i=1}^{N_{traj}} P_n(\cos\theta_i) \quad (2)$$

in which N_{traj} is the total number of the trajectories calculated and θ_i is the polar angle between the initial relative velocity **v** and the final carbon−carbon position vector $\mathbf{r}_{CC}$ of the *i*th trajectory. In each trajectory, the BC molecule would precess about the direction of the final rotational angular momentum **j**. For a near-symmetric top, the precessional frequency could be approximated by $|\mathbf{j}|/2\pi I_m$, in which I_m is the mean value of I_x and I_y. Accordingly, the position vector $\mathbf{r}_{CC}$, and therefore θ_i, would follow the same behavior. To improve the efficiency of the sampling, in the present calculations, the mean value of θ_i, which is an average value over the precessional period of the rotor, was employed in eq 2.

The first and second moments, a_1 and a_2, describe the extents of the orientation and alignment of the final position vector $\mathbf{r}_{CC}$ with respect to the initial relative velocity, respectively. Further higher-order moments were not considered. To have a better understanding of the collision dynamics involved, the changes of the rotational energies and the distributions of the final j_z value were also calculated under various initial collision conditions. Note that, in this report, the j_z value was always taken as the mean value over the molecular precessional period. Because of the finite number of the trajectories, there are always some minor statistical residual moments at asymptotic impact parameter. It was found that a 16 Å or so impact parameter is large enough for this purpose. The asymptotic values of the moments were all reset to 0.0 in this report.

3. Results and Discussions

Orientation of the G Rotamer. As mentioned in the previous section, given a set of translational collision energy and a rotational energy, an allowed angular momentum along the molecular *z* axis and an impact parameter were then selected to define the initial condition of a trajectory. The orientation and alignment moments were calculated accordingly. To cover the collisional conditions in the range from room temperatures to around 1000 K, combinations of four translational collision energies, 0.675, 1.350, 2.700 and 4.050 kcal/mol, with three rotational energies, 0.873, 1.747, and 3.493 kcal/mol, were chosen in this study. Figure 2 shows a typical example of the orientation moment a_1 when the translational collision energy is 2.700 kcal/mol and the molecular rotational energy is 0.873 kcal/mol. As shown in the figure, a specific set of $|j_z|$ values was selected from the range of 0.0−32.4$\hbar$, the allowed values at the selected rotational energy. The corresponding total rotational angular momentum *j* would fall between 80.4$\hbar$ and 32.4$\hbar$. Note that here the classical values, instead of integer

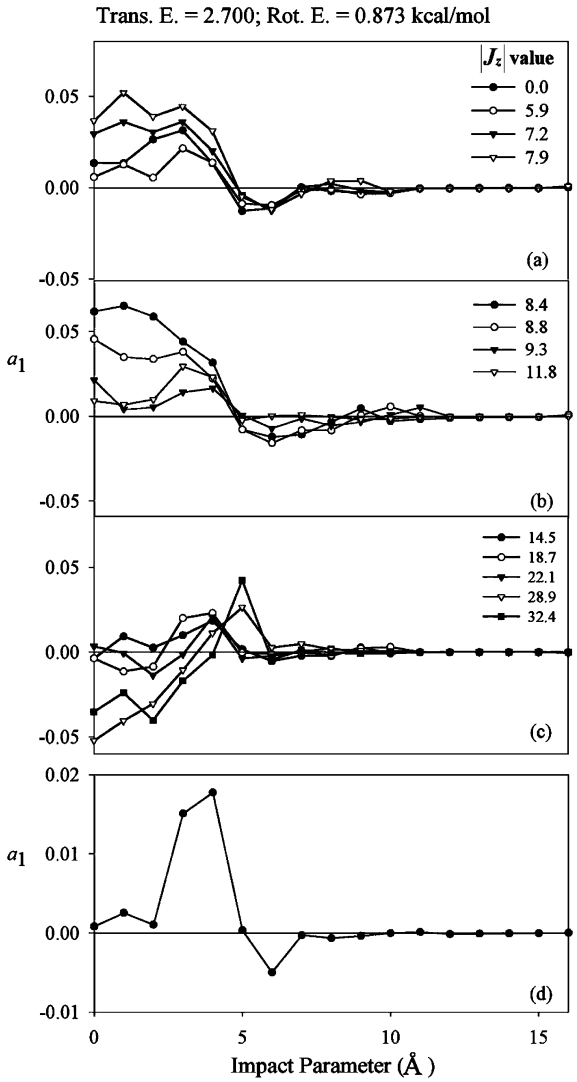

Figure 2. The a_1 orientation moment of the G rotamer as a function of the impact parameter and the j_z value. The initial translational collision energy and rotational energies are 2.700 and 0.873 kcal/mol, respectively. The j_z value is in the unit of $\hbar$. Panel d shows the corresponding spatial-degeneracy-averaged a_1 value.

numbers, were adapted directly. For a given j, the spatial degeneracy would be $2j + 1$. Apparently, for a given initial rotational energy, the contributing weights of higher j_z states to the orientation and alignment moments are less than those with lower j_z values. In the following discussion, the symbol j_z would imply that its absolute value was taken if not being specified otherwise.

Panels a−c of Figure 2 show the a_1 values as a function of the impact parameter. A positive a_1 value indicates that the final $\mathbf{r}_{CC}$ is oriented in the direction of the initial relative velocity, i.e., in the general Ar moving direction, and vice versa. The orientation mainly comes from those collisions with impact parameters being smaller than 5 Å. As shown in the figure, at smaller impact parameter, a positive orientation is obtained for the lower j_z states and a negative one for the higher j_z states. Taking the spatial degeneracy of each j_z state into account, the degeneracy-weighted mean value of a_1 for the selected translational and rotational energies was calculated by summing the degeneracy-weighted a_1 value over the j_z states numerically. The result is shown in panel d of the figure. This suggests that a net positive a_1 value prevails in collisions specified only by the initial translational and rotational energies.

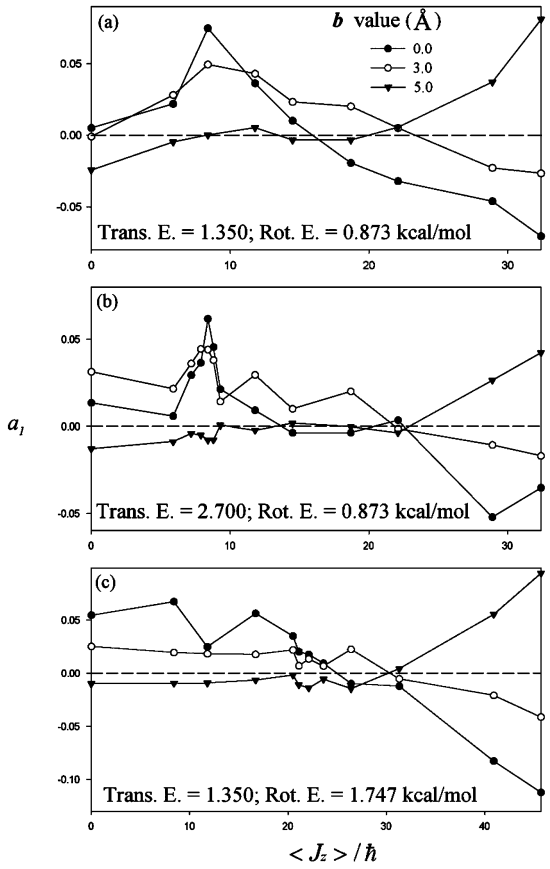

Figure 3. The variation of the a_1 value as a function of j_z at three impact parameters, 0.0, 3.0, and 5.0 Å. Three combinations of translational and rotational energies are examined.

Additional a_1 results in other translational and rotational energies are shown in the Supporting Information section. To have a better general picture of the behavior of a_1, Figure 3 summarizes the variation of the a_1 value as a function of j_z at three important impact parameters, 0.0, 3.0, and 5.0 Å, in three different combinations of collision and rotational energies. All these data suggest that the orientation is strongly dependent on the impact parameter and the j_z value. In the following discussion on this subject, for convenience, a small impact parameter would mean that the impact parameter is smaller than 4 Å. The low j_z states are those states roughly in the lower one-third portion of the maximum allowed j_z value, while the high j_z states indicate those states approximately in the upper one-third j_z group.

Several general patterns emerge from these orientation data. First, at a low j_z state, a_1 is mainly assuming a positive value, while at a high j_z state, it becomes negative at smaller impact parameters but gradually increases to a positive value as the impact parameter increases to around 5 Å. As the figures show, at high j_z states, a_1 shows a positive spike at the impact parameter in the neighborhood of 5 Å. It appears that, for a given rotational energy and within the high j_z states, the peak value of a_1 at around the 5-Å impact parameter increases as the translational collision energy decreases. Second, as shown in panels a and b of Figure 3, if the translational collision energy is larger than the rotational energy, one would note that there are resonance-like features appearing at small impact parameter in the low j_z states. It appears that, the larger the difference between the translational collision energy and the rotational energy gets, the sharper the peak becomes. The peak position is approximately at a j_z value which corresponds to a rotational energy along the molecular z axis being equal to one-fifteenth

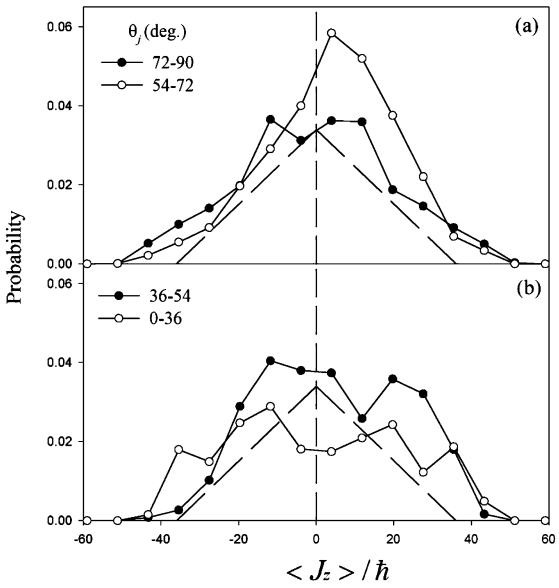

Figure 4. Population distributions of the final j_z classified in four ranges of the final angle of **j**. The total population is normalized to 1. The collisional conditions are: translational collision energy = 1.350 kcal/mol, rotational energy = 0.873 kcal/mol, impact parameter = 0.0 Å, and $|j_z| = 8.4\,\hbar$. The dashed lines are in even distribution and serve as a reference.

of the total rotational energy. For a rotational energy of 0.873 kcal/mol, this j_z value is 8.4ħ. Under this specific rotational energy distribution along the principal axes, the rotational angular velocities along the three molecular principal axes are approximately equal to each other. Apparently, under this collision condition, there is a preferential rotational angular momentum transfer along the molecular *z* axis. On the other hand, if the translational collision energy is close to or less than the rotational energy, the resonance-like enhancement features were not observed. Third, the spatial-degeneracy-weighted a_1 value, as shown in the bottom panels of the related figures, is all dominated by the positive contribution. Finally, the most important observation is that, say within 5 Å of the impact parameter, the cross-section-averaged a_1 value is in the order of 0.01 for these four cases. It is also observed to be true for the other collision conditions considered in this report.

Analysis of the Orientation Effect in the G Rotamer. Since the rotational angular momentum of an isolated system is a space-fixed vector, for a given final rotational angular momentum of the G rotamer, the orientation effect of a molecular-fixed positional vector is directly related to the unequal population distributions in the $\pm|j_z|$ states. In this subsection, the orientation effect results from the collisions with translational collision energy of 1.350 kcal/mol, rotational energy of 0.873 kcal/mol, and initial j_z values of 8.4 and 32.4ħ were specifically studied. The general conclusions could be applied to the other collisional conditions mentioned in this report.

For a given final rotational angular momentum **j**, which is in θ_j angle with respect to the initial relative velocity **v**, one could calculate the corresponding final j_z population distributions. With an initial j_z value of 8.4ħ, the final j_z population distributions classified in four general final **j** directions in the northern sphere, i.e., 0−36, 36−54, 54−72, and 72−90°, are shown in Figure 4. The total population is normalized to 1. Clearly, the j_z states are populated unevenly, especially in the general final directions between 30° and 70°. This results in the preferential orientation of the positional vector $\mathbf{r}_{CC}$ in the direction of **v**. To see how the initial angular momentum ends up in the final rotational

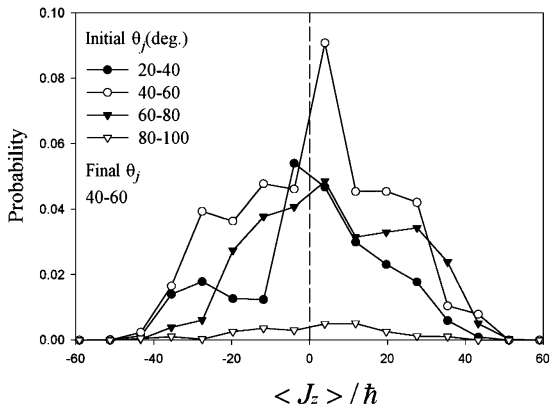

Figure 5. Population distributions of the final j_z classified over the initial collision angles whose final rotational angular momentum **j** ends up in the angles between 40 and 60°. The total population is normalized to 1. The contribution of the other angles not listed in the figure is less than 2%. The collisional conditions are the same as those listed in Figure 4.

angular momentum in the direction range of 40−60°, further analysis was done over the initial rotational angular momentum. Figure 5 shows the relative contributions of the various initial rotational angular momenta that would have a final rotational angular momentum falling in the range of 40−60°. Those angles that are not shown in the figure contribute less than 2% of the total events. The figure shows that the major orientation contribution comes from the collisions with the initial angular momentum being approximately in the range of 40−60°, i.e., in the similar directional range of the final rotational angular momentum. This suggests that the orientation effect mainly comes from the collisions that induce preferential j_z transfers and in the meantime more or less preserve the directions of the initial rotational angular momenta. To facilitate this process, the most effective way is through a torque applied along the molecular *z* axis. This implies that in colliding with Ar, owing to the comparatively larger geometric size and the torque distance with respect to the *z* axis, the $-CH_2Br$ end is more effective in undergoing the j_z momentum transfer than that of the $-CH_2Cl$ end. The net result is the preferential population of the j_z as shown in the figures. Note that for these low initial j_z states, in the molecular coordinates, the direction of the initial angular momentum is close to being perpendicular to the molecular *z* axis. The moment of inertia along the *z* axis is only about one-sixth of the other two moments of inertia. For a given rotational energy change, it would induce the least angular momentum change along the *z* axis. This explains why, in a preferential orientation collision, the directions of the incoming and outgoing rotational angular momenta usually do not undergo drastic change.

As has been mentioned previously, in the high j_z states and at low impact parameters, the orientation effect becomes negative. Taking the extreme case in which the rotation along the *z* axis takes all the available rotational energy as an example, Figure 6 shows the j_z population distributions classified in several final angular momentum directions with respect to the initial relative velocity. With the initial j_z values being fixed at $\pm$32.4ħ, the figure indicates that a comparatively larger portion of the negative j_z states in the neighborhood of $-32.4\,\hbar$ was preserved after the collision. It is especially pronounced in the direction range of 36−72°. This suggests that the orientation effect mainly comes from the collisions that preferentially change the direction of the initial rotational angular momentum. This torque is more effective in being applied to the $-CH_2Cl$

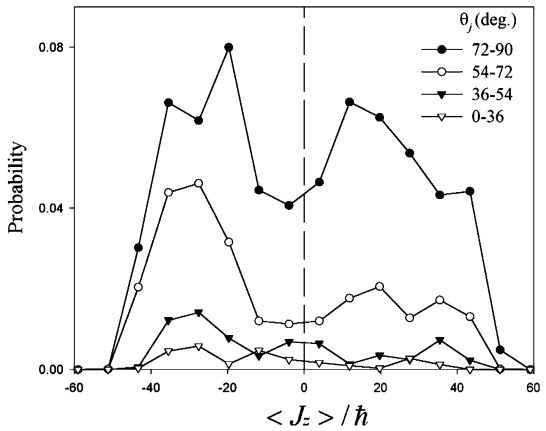

Figure 6. Population distributions of the final j_z classified in four ranges of the final angle of **j**. The total population is normalized to 1. The collisional conditions are the same as those in Figure 4, except that the $|j_z|$ value is set at 32.4ħ, the maximum value allowed by the preset rotational energy.

end than to the $-CH_2Br$ end because the former has a much longer arm to the center of mass of the molecule than that of the latter. The better efficiency in the reorientation of the angular momentum at the $-CH_2Cl$ end would ensure a preferential randomization of the $-CH_2Cl$ end when it directly collides with the Ar atom at small impact parameter. The final net result is a preferential orientation of the $-CH_2Br$ end lying along the direction of the initial relative velocity after the collision.

In contrary of the above situation, under the same high j_z values but with the impact parameter increasing to around 5 Å, the orientation moments become positive. This effect happens in a quite narrow impact parameter range and is more pronounced at lower translational collision energies. With an impact parameter around 5 Å, the van der Waals attractive force between Ar and Br becomes dominant. The result is that the Ar atom simply pulls the $-CH_2Br$ end toward its leaving direction after the collision. This explains the observed positive orientation. The van der Waals attractive force between Ar and Cl, which is expected to be important at an impact parameter around 6 Å, is not strong enough to have an appreciable effect on the orientation moments under the conditions considered in this report. Note that, from the calculations, some minor variations do happen in this impact parameter regime.

In summary, for the G rotamer, with a given translational collision energy and rotational energy, there exists a fixed range of allowable initial j_z states. Taking the contribution of the spatial degeneracy of each j_z state into account, it turns out that the orientation effect is dominated by the low j_z states. The net result is a preferential orientation of the $-CH_2Br$ end lying along the direction of the initial relative velocity after the collision.

Alignment of the G Rotamer. Figure 7 shows the a_2 alignment moments as a function of the impact parameter and the j_z value at translational collision energy of 2.700 kcal/mol and rotational energy of 0.873 kcal/mol, respectively. Panel d of Figure 7 shows the degeneracy-weighted mean alignment moment over the allowed j_z values. Additional a_2 results at other translational and rotational energies are included in the Supporting Information section. Several general trends emerge from these calculations. First, at a smaller impact parameter, the alignment moments of the lower j_z states are generally smaller than those of the higher j_z states, and this trend is independent of the size of the relative energy difference between the translational and rotational energies. At a slightly larger impact parameter around 4 and 5 Å, most alignment moments are

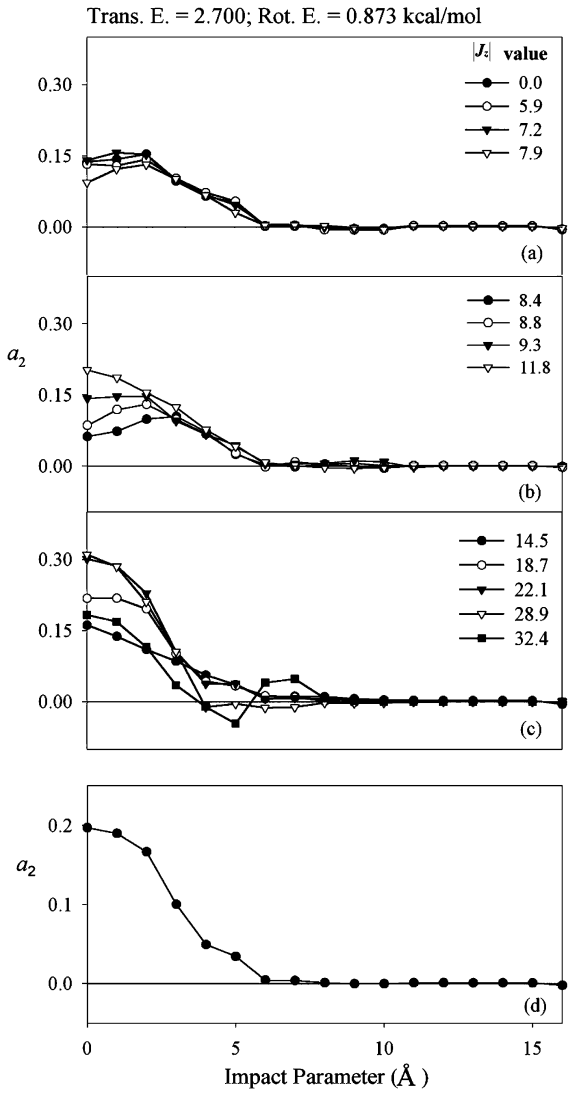

Figure 7. The a_2 alignment moment of the G rotamer as a function of the impact parameter and the j_z value. The initial translational collision energy and rotational energy values are 2.700 and 0.873 kcal/mol, respectively. The j_z value is in the unit of ħ. Panel d shows the corresponding spatial-degeneracy-averaged a_2 value.

positive except for some high j_z states, in which negative alignment values are observed. Second, since the spatial degeneracy of the low j_z states outweighs that of the high j_z states, the final spatial-degeneracy-weighted alignment moment is dominated by the contribution of the low j_z states. Finally, at smaller impact parameters, the spatial-degeneracy-weighted alignment moments are negative if the translational collisional energy is larger than the rotational energy and become positive if the energy order is reverse. For a fixed translational or rotational energy, the larger the energy difference between the translational and rotational energies becomes, the larger the variation of the alignment moment gets. As the impact parameter increases to around 5 Å, a positive alignment moment is always obtained in the energy range considered in this report.

Analysis of the Alignment Effect in the G Rotamer. In the course of modeling the collisional alignment of rotational angular momentum **j** of iodine molecules in supersonic expansion, two types of molecular alignment mechanisms were proposed by Friedrich et al.[10] One alignment mechanism is through a translational relaxation process and is governed by the total collision cross section. This mechanism is more effective in a broad-side collision than an edge-on collision.

Here the broad-side collision means that **j** is nearly parallel with the beam direction, and the edge-on collision indicates that **j** is nearly perpendicular to the beam direction. The molecules with a broad-side collision would suffer more randomization and consequently a preferential alignment of **j** perpendicular to the molecular beam would be observed after the collision. The other mechanism is realized through rotational relaxation. In contrast to the translational relaxation, this process is more effective in an edge-on collision than a broad-side one. A better randomization of the edge-on molecules would result in a preferential alignment of **j**, which is parallel with the molecular beam.[10] Note that, for a linear molecule, the rotational angular momentum alignment moment and the alignment moment of the position vector along the internuclear axis are related with each other in opposite sign.[10] For the present molecular system, it has been noticed that the low j_z states would determine the final net alignment effect after collision. The rotational motion of these low j_z states could be qualitatively pictured as that of a linear molecule if the precessional motion is neglected. In other words, the basic alignment physical picture obtained for the linear molecules could be applied to the present near-symmetric top in the low j_z states. In the following discussion, we shall adapt the above general mechanisms developed for the alignment effect of the linear molecules to elucidate the present theoretical results of a near-symmetric top.

Figure 8 shows the probability distributions of the rotational energy changes with a translational collision energy of 2.700 kcal/mol and rotational energies of 0.873, 1.747, and 3.493 kcal/mol, respectively. The impact parameters are all set at 2 Å. The j_z values are set at 18.7, 26.4, and 37.4$\hbar$, values that correspond to the conditions in which one-third of the rotational energies are allocated equally along each of the three molecular principal axes. Panels a−c of Figure 8 show the probability distributions of the changes of rotational energy with the initial relative velocity being either perpendicular to or parallel with the initial rotational angular momentum. The parallel collisions are defined as those with the collision angles being within 20° of 0 or 180° and the perpendicular ones being within ±10° of 90°. Panel d shows the overall probability distributions of the rotational energy changes.

The general features of these probability distributions could be rationalized straightforwardly by the alignment mechanisms mentioned above. Panel d of the figure clearly shows that, as the translational collision energy is larger than the rotational energy, there is a net transfer of energy from the former form to the latter form and vice versa. In other words, the translational relaxation process is dominated in the collision process if the translational energy is larger than the rotational energy and vice versa. To further identify the major contributing channel for these two relaxation processes, panels a and b show that, in the translational-relaxation-dominated collisions, the encounters with **j** that are parallel with the initial relative velocity are more effective. On the other hand, for the rotational-relaxation-dominated collision, as shown in panel c, the encounters with **j** that are perpendicular to the relative velocity become more efficient. In summary, at a small impact parameter, if the translational energy is larger than the rotational energy, **j** would be aligned perpendicularly to the relative velocity. This implies that the positional vectors which are close to the molecular *z* axis would be aligned parallelly with the relative velocity. One would expect a positive alignment moment for the positional vector. Following the same argument, a negative alignment moment for the positional vector is expected for the rotational relaxation process.

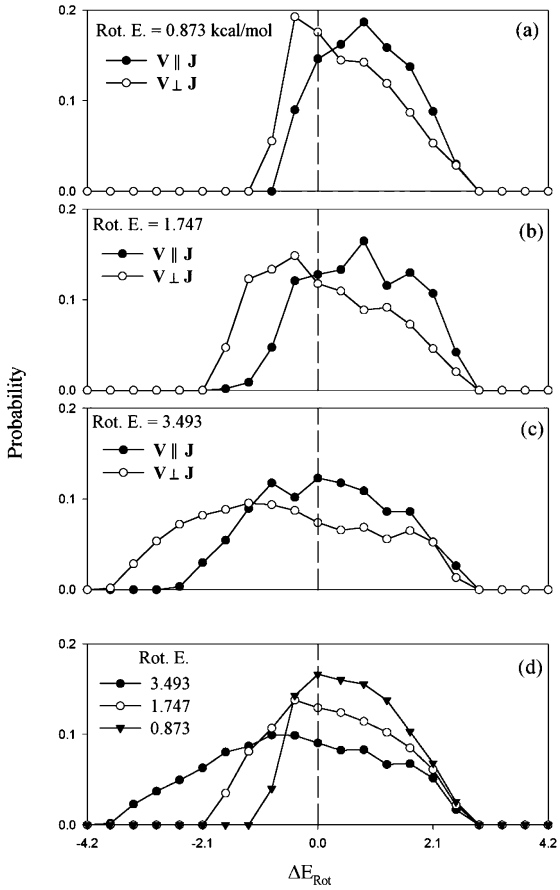

Figure 8. The population distributions of the changes of the rotational energy at three initial rotational energies, 0.873, 1.747, and 3.493 kcal/mol, respectively. The initial translational collision energy is all set at 2.700 kcal/mol. The initial $|j_z|$ values are set at 18.7, 26.4, and 37.4$\hbar$, respectively, which is corresponding to one-third of the total rotational energy being allocated to the molecular *z* axis. The impact parameter is 2 Å. Panels a−c show the distributions with the collisions being either perpendicular or parallel to the initial rotational angular momentum **j**. Panel d shows the distributions of the overall collisions at three rotational energies.

As the impact parameter increases to around 4 or 5 Å, the broad-side encounters, which have a larger collision cross section, would always dominate the whole collision process and a positive alignment moment was always obtained. The consequence is that, at high impact parameters, the spatial-degeneracy-averaged alignment moment is only weakly dependent on the translational and rotational energies.

Orientation of the T Rotamer. Figure 9 shows the orientation moment a_1 of the T rotamer at translational collision energy of 1.350 kcal/mol and rotational energy of 0.863 kcal/mol. Additional a_1 results of the T rotamer at other rotational and translational collisional energies are included in the Supporting Information section. In contrast to the G rotamer case, the spatial-degeneracy-weighted a_1 values of the T rotamer mainly come from higher-impact parameter collisions and result in oscillatory behavior. As the impact parameter varies from 3.5 to 6.5 Å, the a_1 could swing from negative to positive and then come back to a negative value or close to baseline. The relative peak heights of these oscillations vary as the initial translational and rotational energies change. Through one way or another, all the j_z states contribute to the final spatial-degeneracy-averaged a_1 value. In other words, for the T rotamer, the spatial-degeneracy-averaged a_1 moment is not dominated by specific j_z states. Following the general argument developed for the G rotamer case, one could rationalize the characteristic features

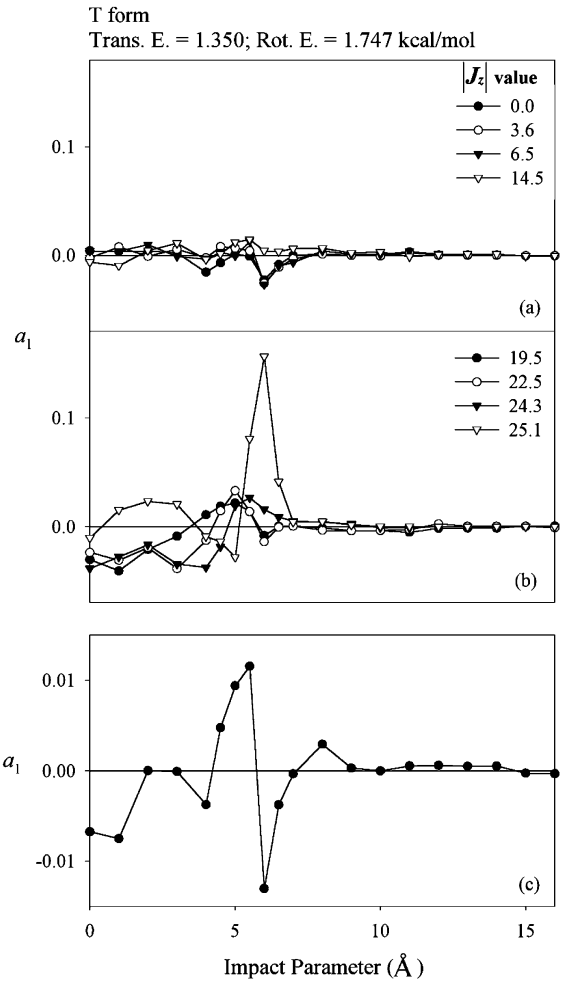

Figure 9. The a_1 orientation moment of the T rotamer as a function of the impact parameter and the j_z value. The initial translational collision energy and rotational energy values are 1.350 and 1.747 kcal/mol, respectively. The j_z value is in the unit of $\hbar$. Panel c shows the corresponding spatial-degeneracy-averaged a_1 value.

of the T rotamer as follows. The distances of the chlorine and bromine atoms to the center of mass of the T rotamer are 2.91 and 1.56 Å, respectively. With the van der Waals radii of Ar, Cl, and Br to be 1.99, 2.07, and 2.22 Å, respectively, in the present potential functional form of exponential repulsion and attraction, one would expect that, at impact parameters around 4, 5, and 6 Å, the collisions that contribute to the observed orientation effect would be corresponding to direct collisions with the chloro end, glancing collisions in the bromo end, and finally glancing collisions in the chloro end, respectively. For the direct collision with the chloro end, a preferential transfer of momentum along the molecular *z* axis and also the randomization reorientation of the total angular momentum result in a negative orientation effect. In the case of the glancing collision in the bromo end, through the van der Waals attractive force between Ar and Br, the bromo end would follow the outgoing Ar and a positive orientation effect is expected. With the same argument, a reverse orientation effect would be observed for the glancing collision in the chloro end. Following these physical interpretations, one could anticipate three general behavior trends for these three orientation channels. They are described as follows. First, because the van der Waals attractive interaction of Br/Ar is stronger than that of Cl/Ar, the positive orientation effect at 5 Å is expected to be more pronounced than the negative one at 6 Å. Second, at a fixed initial rotational energy, the higher the initial translational collision energy gets, the less the orientation effect of the glancing collisions becomes, and in the meantime, the more pronounced the orientation effect of the direct collisions in the chloro end becomes. Third, if the rotational energy is comparable or larger than the translational energy, the rotational energy relaxation would become more important in a direct collision. The consequence is that, for those direct collisions at impact parameter around 4 Å, the angular momentum transfer process that could eventually result in the preferential orientation for the chloro end is getting less effective. In other words, the negative orientation effect at this impact parameter would get less pronounced as the rotational energy is comparable or larger than the translational collision energy.

One could clearly see the manifestation of the above effects in Figure 9 and also in Figures s26 and s29 of the Supporting Information section. In these cases, the rotational energy is fixed at 1.747 kcal/mol and the translational energy is varied from 1.350 to 4.050 kcal/mol. The figures indicate that the negative orientation effect at 4 Å increases, and both the positive orientation effect at 5 Å and negative orientation effect at 6 Å decrease according to the variation of the translational energies. In the case of 1.747-kcal/mol rotational energy and 1.350-kcal/mol translational energy, a model example in which the rotational energy is larger than the translational energy, the negative orientation effect at 4 Å is negligibly small. This phenomenon could be observed easily in Figure 9.

These results, along with the additional data in the Supporting Information section, suggest that the orientation effect of the T rotamer is heavily dependent on the translational and rotational energies. The overall orientation effect could be varied from a net negative effect to a net positive effect by changing the translational and rotational energies. This is in sharp contrast to the case of the G rotamer in which a consistent positive orientation effect is found throughout the whole energy range studied in this report. Nevertheless, even for the most favorable cases in the T rotamer, their net orientation effect is at best only comparable with the G rotamer. Under most collisional conditions considered in this report, their net orientation effect is negligibly small. Overall, the T rotamer is oriented in a much less degree than the G rotamer in colliding with an Ar atom. It is simply because the T rotamer has a more extended and symmetric geometric structure, a preferential collisional transfer of the angular momentum along the molecular *z* axis as discussed in the G rotamer case is just less effective in the T rotamer.

Alignment of the T Rotamer. Figure 10 shows the alignment moment a_2 of the T rotamer at translational energy of 2.700 kcal/mol and rotational energy of 0.873 kcal/mol. Additional a_2 moments of the T rotamer at other translational and rotational energies are included in the Supporting Information section. Comparing these T rotamer a_2 data with those of the G rotamer with the same translational and rotational energies, one finds that the spatial-degeneracy-averaged a_2 values of these two rotamers are closely resembled to each other. Setting aside their differences in the absolute magnitudes, the general behaviors of the alignment moments of the individual j_z states between the counterparts of these two rotamers are also similar to each other. In short, the alignment mechanisms and the general conclusions obtained earlier for the G rotamer could be carried over to the present T rotamer case without modifications.

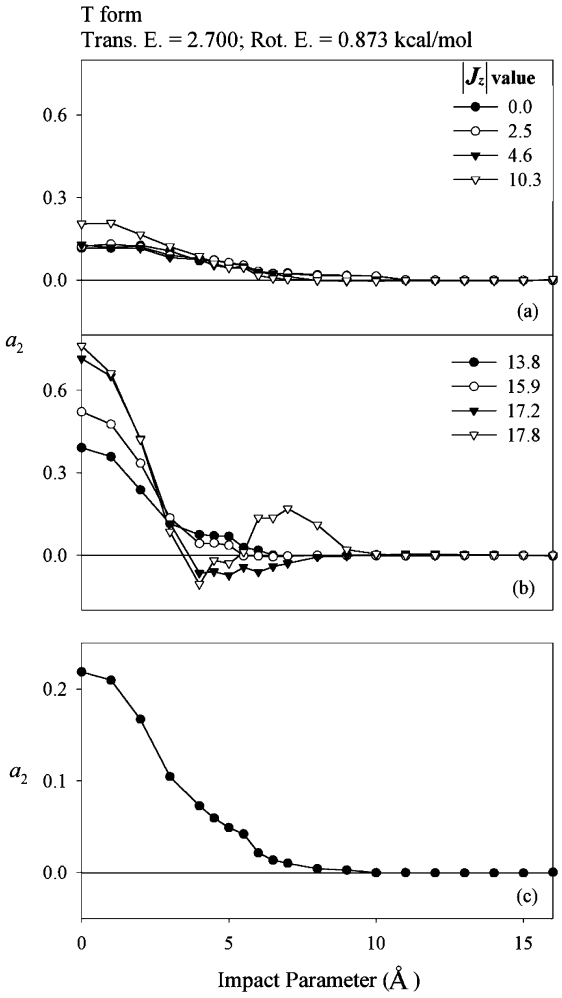

Figure 10. The a_2 alignment moment of the T rotamer as a function of the impact parameter and the j_z value. The initial translational collision energy and rotational energy values are 2.700 and 0.873 kcal/mol, respectively. The j_z value is in the unit of $\hbar$. Panel c shows the corresponding spatial-degeneracy-averaged a_2 value.

4. Conclusion

The collisional orientation and alignment moments of the carbon−carbon bond vector of the G and T rotamers of 1-bromo-2-chloroethane in colliding with an argon atom were studied theoretically under various collision conditions. There is a robust manifestation of the collisional orientation for the G rotamer. Under single-collision conditions, this effect may be not that dramatic. Nevertheless, in a directed flow, a sequence of collisions would provide an opportunity in enhancing the effect, as has been demonstrated experimentally and theoretically in a supersonic molecular beam expansion situation. Under the collision conditions considered in this report, much less net orientation effect was obtained for the T rotamer. On the other hand, it is shown that the alignment behaviors of the T and G rotamers are similar to each other. In contrast to the orientation effect, the alignment effect is heavily dependent on the size of the relative energy difference between the translational collision energy and rotational energy. General orientation and alignment mechanisms were proposed to rationalize the observations of the theoretical calculation results.

Acknowledgment. The financial support of this work by the National Science Council, Taipei, Taiwan, is gratefully acknowledged.

Supporting Information Available: One table that lists the constant parameters adapted in the force field of the BC + Ar system and 38 figures that include the additional orientation and alignment moments of the G and T rotamers under various translational and rotational energies considered in report. This material is available free of charge via the Internet at http://pubs.acs.org.

References and Notes

(1) McCourt, F. R. W.; Beenakker, J. J. M.; Kohler, W. E.; Kuscer, I. *Nonequilibrium Phenomena in Polyatomic Gases, Volume 1: Dilute Gases*; Oxford University Press: Oxford, 1990.
(2) Sinha, M. P.; Caldwell, C. D.; Zare, R. N. *J. Chem. Phys.* **1974,** *61,* 491.
(3) Sanders W. R.; Anderson, J. B. *Chem. Phys. Lett.* **1977,** *47,* 283.
(4) Sanders W. R.; Anderson, J. B. *J. Phys. Chem.* **1984**, *88*, 4479.
(5) Hefter, U.; Ziegler, G.; Mattheus, A.; Fischer, A.; Bergmann, K. *J. Chem. Phys.* **1986,** *85,* 286.
(6) Dressler, R. A.; Meyer, H.; Leone, S. R. *J. Chem. Phys.* **1987,** *87,* 6029.
(7) Pullman, D. P.; Herschbach, D. R. *J. Chem. Phys.* **1989,** *90,* 3881.
(8) Pullman, D. P.; Friedrich, B.; Herschbach, D. R. *J. Chem. Phys.* **1990,** *93,* 3224.
(9) Hulsman, H.; Korving, J. *J. Chem. Phys.* **1991,** *95,* 5719.
(10) Friedrich, B.; Pullman, D. P.; Herschbach, D. R. *J. Phys. Chem.* **1991,** *95,* 8118.
(11) Saleh, H. J.; McCaffery, A. J. *J. Chem. Soc., Faraday Trans.* **1993,** *89,* 3217.
(12) Weida, M. J.; Nesbitt, D. J. *J. Chem. Phys.* **1994,** *100,* 6372.
(13) Aquilanti, V.; Ascenzi, D.; Cappelletti, D.; Pirani, F. *Nature* **1994,** *371,* 399.
(14) Aquilanti, V.; Ascenzi, D.; Cappelletti, D.; Franceschini, S.; Pirani, F. *Phys. Rev. Lett.* **1995,** *74,* 2929.
(15) Pullman, D. P.; Friedrich, B.; Herschbach, D. R. *J. Phys. Chem.* **1995,** *99,* 7407.
(16) Anthony, E. B.; Schade, W.; Bastian, M. J.; Bierbaum, V. M.; Leone, S. R. *J. Chem. Phys.* **1997,** *106,* 5413.
(17) Harich, S.; Wodtke, A. M. *J. Chem. Phys.* **1997,** *107,* 5983.
(18) Aquilanti, V.; Ascenzi, D.; Cappelletti, D.; Fedeli, R.; Pirani, F. *J. Phys. Chem. A* **1997,** *101,* 7648.
(19) Aquilanti, V.; Ascenzi, D.; de Castro Vitores, M.; Pirani, F.; Cappelletti, D. *J. Chem. Phys.* **1999,** *111,* 2620.
(20) Fair, J. R.; Nesbitt, D. J. *J. Chem. Phys.* **1999,** *111,* 6821.
(21) Pirani, F.; Cappelletti, D.; Bartolomei, M.; Aquilanti, V.; Scotoni, M.; Vescovi, M.; Ascenzi, D.; Bassi, D. *Phys. Rev. Lett.* **2001,** *86,* 5035.
(22) Pirani, F.; Bartolomei, M.; Aquilanti, V.; Scotoni, M.; Vescovi, M.; Ascenzi, D.; Bassi, D.; Cappelletti, D. *J. Chem. Phys.* **2003,** *119,* 265.
(23) Aquilanti, V.; Ascenzi, D.; Cappelletti, D.; de Castro, M.; Pirani, F. *J. Chem. Phys.* **1998,** *109,* 3898.
(24) Frisch, M. J.; Trucks, G. W.; Schlegel, H. B.; Scuseria, G. E.; Robb, M. A.; Cheeseman, J. R.; Zakrzewski, V. G.; Montgomery, J. A., Jr.; Stratmann, R. E.; Burant, J. C.; Dapprich, S.; Millam, J. M.; Daniels, A. D.; Kudin, K. N.; Strain, M. C.; Farkas, O.; Tomasi, J.; Barone, V.; Cossi, M.; Cammi, R.; Mennucci, B.; Pomelli, C.; Adamo, C.; Clifford, S.; Ochterski, J.; Petersson, G. A.; Ayala, P. Y.; Cui, Q.; Morokuma, K.; Malick, D. K.; Rabuck, A. D.; Raghavachari, K.; Foresman, J. B.; Cioslowski, J.; Ortiz, J. V.; Stefanov, B. B.; Liu, G.; Liashenko, A.; Piskorz, P.; Komaromi, I.; Gomperts, R.; Martin, R. L.; Fox, D. J.; Keith, T.; Al-Laham, M. A.; Peng, C. Y.; Nanayakkara, A.; Gonzalez, C.; Challacombe, M.; Gill, P. M. W.; Johnson, B. G.; Chen, W.; Wong, M. W.; Andres, J. L.; Head-Gordon, M.; Replogle, E. S.; Pople, J. A. *Gaussian 98*, revision A.9; Gaussian, Inc.: Pittsburgh, PA, 1998.
(25) Hase, W. L. et. al. *Venus96*; Wayne State University: Detroit MI, 1996.
(26) Allinger, N. L. et al. *MM3(94)*; University of Georgia: Athens, GA, 1994.
(27) Vande Linde, S. R.; Hase, W. L. *J. Phys. Chem.* **1990**, *94*, 2778.
(28) Wang, H.; Zhu, L.; Hase, W. L. *J. Phys. Chem.* **1994**, *98*, 1608.